https://doi.org/10.5194/egusphere-2023-2251
Preprint. Discussion started: 24 October 2023
© Author(s) 2023. CC BY 4.0 License.

The characteristics of tides and their effects on the general circulation of the Mediterranean Sea

Bethany McDonagh[1,2], Emanuela Clementi[1], Anna Chiara Goglio[1], and Nadia Pinardi[2]

[1]Centro Euro-Mediterraneo sui Cambiamenti Climatici – CMCC, Italy
[2]Department of Physics and Astronomy, University of Bologna, Italy

Correspondence: Bethany McDonagh (beth.mcdonagh@unibo.it), Emanuela Clementi (emanuela.clementi@cmcc.it)

Abstract. The effects of tides on the Mediterranean Sea's general circulation, with a particular focus on the horizontal and vertical currents, are investigated using twin simulations with and without tides. Amplitudes of tides in the region are typically low, but an analysis of the kinetic energy demonstrates that tides have effects across many spatial and temporal scales in the basin, including nonlinear effects at short periods (less than one day) with high kinetic energy peaks at near-inertial, basin modes and tidal frequencies. Internal tidal waves are also revealed below 100m. Tides are found to amplify several basin modes of the Mediterranean Sea, broaden several tidal frequency energy spectra bands, as well as interact energetically with near-inertial waves. Tides are found to increase the mixed layer depth in the Mediterranean Sea, particularly in the deep and intermediate water formation areas of the Western and Eastern basins. It is confirmed that the net mass transport through the Gibraltar Strait is unchanged by tides, but both inflow and outflow increase.

1 Introduction

Tidal forcing is a rather recent addition to large scale circulation models that start to have horizontal and vertical resolutions that allow for an analysis of tidal motion on the circulation. For an overall review of the topic, see Arbic (2022). Tides are now considered to be essential components of the large scale circulation, their global average input energy is 3.5TW (Simmons et al., 2004), the second largest after winds (Ferrari and Wunsch, 2010), and they generate internal tides that then drive internal mixing (de Lavergne et al., 2020).

For the Mediterranean Sea, several authors have depicted the importance of tidal motion for the Gibraltar Strait (Armi and Farmer, 1985; Candela et al., 1990; Harzallah et al., 2016). Recently, Gonzalez (2023) has revisited the tidal dynamics in the Gibraltar Strait, concluding that there are several tidal-induced hydraulic control points and the authors developed a specific mixing parametrization for the Strait. Harzallah et al. (2016) and Naranjo et al. (2014) found that tides at the Strait of Gibraltar: (1) increase the baroclinic volume transport, (2) increase the salinity of Atlantic inflowing waters through the enhancement of mixing, affecting the water mass formation processes further downstream from the Strait and (3) change the Mediterranean deep water outflow.

Recently, observational and modelling studies have also started to advance our understanding of internal tides in several regions of the Mediterranean Sea. Diurnal internal tide oscillations are generated around the Adriatic Sea islands in observational

https://doi.org/10.5194/egusphere-2023-2251
Preprint. Discussion started: 24 October 2023
© Author(s) 2023. CC BY 4.0 License.

studies (Mihanović et al., 2009), leading to baroclinic trapped waves. In a recent paper, Oddo et al. (2023) found observational and modelling evidence of internal tides at the Sicily-Malta escarpment due to the diurnal tidal components, connected to the bathymetric gradients.

Internal tides are characterised by relatively large vertical velocities with respect to the Ekman suction and pumping, while their horizontal wavelength is similar to the general circulation scales (Oddo et al., 2023). In the North Atlantic, the addition of tides was found to improve the representation of the mixed layer depth and deep water formation in the Labrador Sea (Müller et al., 2010). Lee et al. (2006) found that in the same region, sea surface density was increased by the addition of tides to their model and found that this could enhance ventilation and overturning. Internal wave frequencies around 8 hours were also found by van Haren et al. (2014) in the northwestern Mediterranean Sea.

Other features of the Mediterranean Sea that bear importance when discussing tides are the free barotropic oscillations induced by atmospheric pressure and wind forcing. The Mediterranean Sea's first barotropic basin mode is at 38.5 hours (Schwab and Rao, 1983), beyond that of semidiurnal tides, but modes also exist at 11.4, 8.4, and 7.4 hours (Schwab and Rao, 1983), and 8 hours (Lamy et al., 1981; Lozano and Candela, 1995). Many of these free oscillations could be affected or enhanced by tides, especially considering their proximity to tidal frequencies. The Adriatic Sea is characterised by seiches or free barotropic oscillations close to tidal frequencies: at 10.7 hours and 21.9 hours (Medvedev et al., 2020; Leder and Orlić, 2004; Schwab and Rao, 1983), and at 12.0 hours (Lozano and Candela, 1995).

In this work, we further characterise the tidal large scale circulation effects in the overall Mediterranean Sea. To do this, we analyse the differences between a general circulation ocean model with and without tides, focusing on changes in the spectra, in the horizontal and vertical dynamics both across the basin on average and in several water mass formation regions. Furthermore, we show the impact of tides in the Eastern Mediterranean Sea and the amplification of different basin modes by a tidal resonant mechanism.

In the Mediterranean Sea there are four key regions of deep and intermediate water formation (see Figure 1): the Gulf of Lion (Western Mediterranean Deep Water, WMDW) and South Adriatic (Eastern Mediterranean Deep Water, EMDW) for deep water formation, and the Cretan Sea (Cretan Deep Water, CDW, and Cretan Intermediate Water, CIW) and Rhodes Gyre (Levantine Deep Water, LDW, and Levantine Intermediate Water, LIW) for intermediate water formation (Pinardi et al., 2015). In these regions the vertical velocities are enhanced, and this paper will analyse in detail the differences of water mass formation rates with and without tides.

Section 2 describes the model and observational data used and the analysis methods, while Sections 3-8 contain the model results and conclusions as follows:

- Section 3: Sea level energy spectra
- Section 4: Kinetic energy spectra
- Section 5: Mixed layer depth and water mass formation
- Section 6: Temperature and salinity

https://doi.org/10.5194/egusphere-2023-2251
Preprint. Discussion started: 24 October 2023
© Author(s) 2023. CC BY 4.0 License.

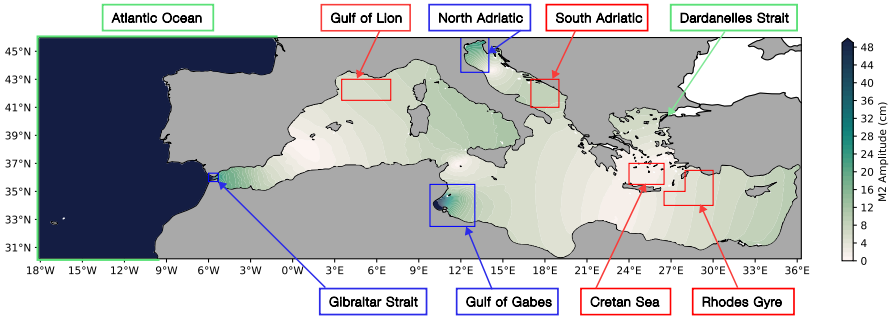

Figure 1. Map of the M2 tidal component amplitude (contours) in the Mediterranean Sea, with highlighted regions of open ocean dense water formation in red, regions with high tidal amplitude in blue and lateral open boundary conditions from the model configuration (see Section 2) in green.

- Section 7: The Gibraltar Strait
- Section 8: Conclusions

2 Data and methods

The general circulation model used is NEMO v3.6, following the implementation of the Mediterranean Sea forecasting system operational in the framework of the Copernicus Marine Service (Coppini et al., 2023; Clementi et al., 2021). The area covered by the model is shown in Fig. 1.

The model has $\frac{1}{24}^\circ$ uniform horizontal resolution with 141 uneven vertical levels, using z* vertical coordinates and partial steps. This model is eddy-resolving, since the Rossby radius of deformation is of the order of 10km in the Mediterranean and the horizontal resolution of the model is approximately 4km. Atmospheric forcing fields are given by the six-hour European Centre for Medium-Range Weather Forecasts (ECMWF) analyses, at a horizontal resolution of $\frac{1}{8}^\circ$ (2015-2018) and $\frac{1}{10}^\circ$ (2019-2021) and they are used to compute momentum, water and heat fluxes using specifically designed bulk formulae (Pettenuzzo et al., 2010). Lateral open boundary conditions are used in the Atlantic Ocean and Dardanelles Strait (see Fig. 1). Additionally, monthly mean climatological freshwater inputs from 39 rivers are added to the surface layer. The bathymetry used is the GEBCO 30-sec bathymetry (GEBCO Bathymetric Compilation Group 2014, 2014), interpolated onto the model grid.

In the chosen configuration, vertical diffusivity depends on the Richardson number, calculated according to Pacanowski and Philander (1981). The Richardson number is a ratio of buoyancy to horizontal shear:

$$Ri = \frac{N^2}{\frac{\partial \bar{v}}{\partial z}^2} \tag{1}$$

https://doi.org/10.5194/egusphere-2023-2251
Preprint. Discussion started: 24 October 2023
© Author(s) 2023. CC BY 4.0 License.

Tidal component	Period (hours)	Description
M2	12.421	Principal lunar semidiurnal tidal constituent
S2	12.000	Principal solar semidiurnal tidal constituent
K1	23.934	Lunisolar diurnal tidal constituent
O1	25.819	Lunar diurnal tidal constituent
N2	12.658	Larger lunar elliptic semidiurnal tidal constituent
P1	24.066	Solar diurnal tidal constituent
Q1	26.868	Larger lunar elliptic diurnal tidal constituent
K2	11.967	Lunisolar semidiurnal tidal constituent

Table 1. Tidal constituent components used in the model for this work, with their respective periods and astronomical descriptions.

where N^2 is the Brunt-Väisälä frequency, and $\frac{\partial \bar{v}}{\partial z}^2$ is the horizontal shear. Enhanced vertical viscosity and diffusivity are used where layers are unstable ($N^2 \leq -1 \times 10^{-12}$ s^{-2}) imposing a vertical diffusivity coefficient of 10 m^{2}s^{-1}. Vertical viscosity and diffusivity are then calculated according to:

$$A^{vT} = \frac{A^{vT}_{ric}}{(1+aRi)^n} + A^{vT}_b \tag{2}$$

$$A^{vm} = \frac{A^{vT}}{(1+aRi)} + A^{vm}_b \tag{3}$$

where A^{vT} and A^{vm} are the vertical eddy viscosity and diffusivity respectively, and A^{vT}_{ric}, a, and n are adjustable parameters. In the model runs used, these values are 100×10^{-4} m^{2}s^{-1}, 5, and 2 respectively. Background vertical eddy diffusivity and vertical eddy viscosity values are $A^{vT}_b = 10^{-7}$ m^{2}s^{-1} and $A^{vm}_b = 1.2 \times 10^{-6}$ m^{2}s^{-1} respectively.

Twin experiments are presented in this work with and without the representation of tides. In the experiments including tides, the 8 major tidal components for the Mediterranean Sea (M2, S2, K1, O1, N2, Q1, K2, P1) are represented, which are detailed further in Table 1. The M2 amplitude is displayed in Fig. 1 showing the well-known high amplitude areas at the Gibraltar Strait, the Gulf of Gabes and the Northern Adriatic Sea. Moreover, the Atlantic Ocean lateral open boundary fields include tidal forcing from TPXO9 (Egbert and Erofeeva, 2002).

Other than the addition of the tidal forcing itself, there are some other differences between the tidal and non-tidal modelling set-ups (see Table 2), with the primary difference being the time integration method. Both experiments use a split-explicit free surface formulation proposed in Shchepetkin and McWilliams (2005), solving the free surface equation and the associated barotropic velocity equations with a smaller timestep than the one used for the three-dimensional prognostic variables. The non-tidal experiment uses forward time integration, in which the external mode (barotropic timestep) is integrated between the current and the subsequent baroclinic time steps. This was not stable in the experiment including tides, so this instead uses a centred integration scheme, where the baroclinic to barotropic forcing term given at the actual time step becomes centred in

https://doi.org/10.5194/egusphere-2023-2251
Preprint. Discussion started: 24 October 2023
© Author(s) 2023. CC BY 4.0 License.

	Experiment without tides	Experiment with tides
Timestep	240s	120s
Time integration scheme	Forward	Centred
Tides	No tidal forcing	8 tidal components: M2, S2, K1, O1, N2, P1, Q1, K2
Boundary conditions	No tidal signal at the boundary	Additional tidal signal at the Atlantic boundary: horizontal currents and sea surface height
Bathymetry	GEBCO 2014 interpolated onto model grid	Topography changed in 3 grid points at the boundary in the Bay of Biscay and 4 grid points in the Adriatic Sea

Table 2. Summary of the key differences between the tidal experiment and the experiment without tides.

the middle of the integration window. The tidal experiment uses a shorter timestep, 120s, rather than 240s in the experiment without tides, which was changed for stability purposes. The bathymetry was adjusted at several points in the tidal experiment for stability reasons: in the Bay of Biscay, at the northernmost part of the model domain, and several points were modified along the Croatian coastline to avoid generation of spurious tidal signals due to islands and complex bathymetry. All of the above changes in the tidal model are implemented as in Agresti (2018).

The model was integrated starting from climatological temperature and salinity initial conditions for seven years (2015-2021), with the first two years removed from the following analysis and considered as a spin-up period.

3 Sea level energy spectra

A spectrum of hourly sea surface height (SSH) in the Mediterranean Sea for five years is shown in Fig. 2 for both tidal and non-tidal experiments. The diurnal and semidiurnal tidal components represent the major differences between the two solutions, as expected. Further differences between the two models away from these tidal frequencies are also visible. Tides appear to modulate the spectrum at the mesoscales: energy is reduced in the tidal model at frequencies lower than 0.5 d^{-1} (longer than a period of two days).

Peaks at both 24 hours and 12 hours are apparent, both with and without tides. In the case without tides, the energy peaks can be attributed to basin modes excited by atmospheric pressure forcing, as found by Oddo et al. (2014) using a similar NEMO configuration. In the semidiurnal range, the tidal model introduces a broad peak around 12 hours, as well as peaks at the individual tidal component frequencies. This is due to the amplification by tides of the basin modes near and at these frequencies. We argue that the broad 12h energy peak in Figure 2 in the tidal run is composed of the amplified 11.4h Mediterranean Sea basin mode energy (Schwab and Rao, 1983), the first Adriatic mode at 10.7h, known to be enhanced by tides (Medvedev et al., 2020; Schwab and Rao, 1983), and the 12h Adriatic/Aegean seas mode (Lozano and Candela, 1995). Peaks are also seen at 8h

https://doi.org/10.5194/egusphere-2023-2251
Preprint. Discussion started: 24 October 2023
© Author(s) 2023. CC BY 4.0 License.

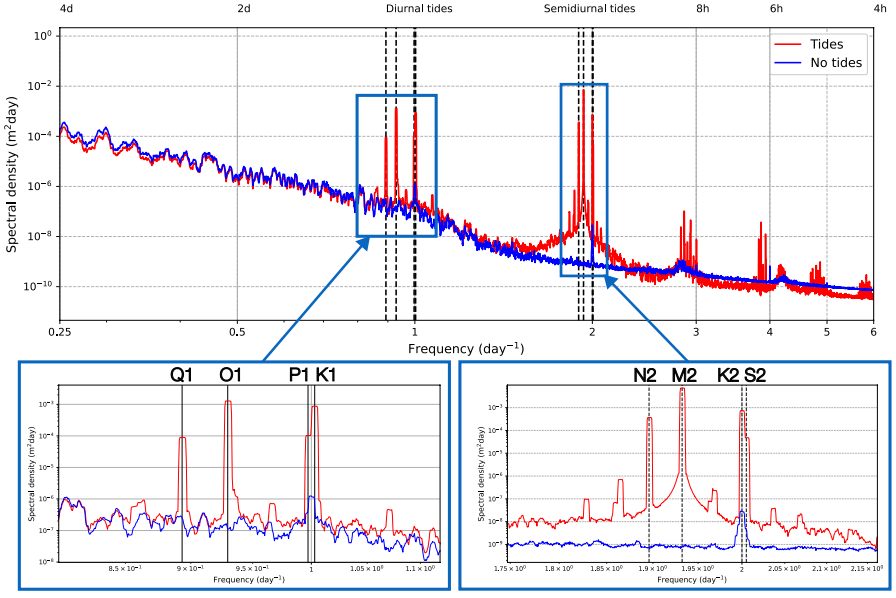

Figure 2. Energy density spectrum of hourly mean sea surface height in the Mediterranean Sea for the period 2017-2021, for the experiment without tides (blue) and with tides (red). Boxes below the figure show the key diurnal and semidiurnal ranges to highlight the representation of each individual tidal component.

and 6h, which correspond to the kinetic energy frequencies noted in the Sicily Strait by Palma et al. (2020), and in their work, these peaks were considered to come from non-linear effects of tides. The peak at 8h also aligns with the Western Mediterranean basin mode of 8.4h discussed in Schwab and Rao (1983). Schwab and Rao (1983) also noted a fourth Mediterranean mode at 7.4h and the third Adriatic mode at 6.7h, which align with some of the higher frequency peaks in Fig. 2. Lozano and Candela (1995) discussed an 8.2h mode in the Gulf of Gabes, which also could contribute to this peak.

Considering the amplification of basin modes, sea level spectra in the Adriatic Sea and Gulf of Gabes are shown in Fig. 3, to understand whether the peaks in Fig. 2 correspond to modes in these regions. In the Adriatic Sea (Fig. 3a), the sea level energy peaks at the frequencies of the barotropic modes of the Adriatic Sea at 11.4 hours, 6.7 hours (Schwab and Rao, 1983) and 12 hours (Lozano and Candela, 1995), are all enhanced by tides. The peaks are also visible in the model without tides, but with lower energy, thus confirming that these peaks are due to amplification of modes forced by winds and atmospheric pressure. In the Gulf of Gabes (Fig. 3b), the mode at 8.2 hours (Lozano and Candela, 1995) is also enhanced by tides.

4 Kinetic energy spectra

For this analysis, several points were selected across the Mediterranean Sea, to understand the effects of tides on local phenomena such as the generation of internal tides and interactions with near-inertial waves. A map of these points is shown in

https://doi.org/10.5194/egusphere-2023-2251
Preprint. Discussion started: 24 October 2023
© Author(s) 2023. CC BY 4.0 License.

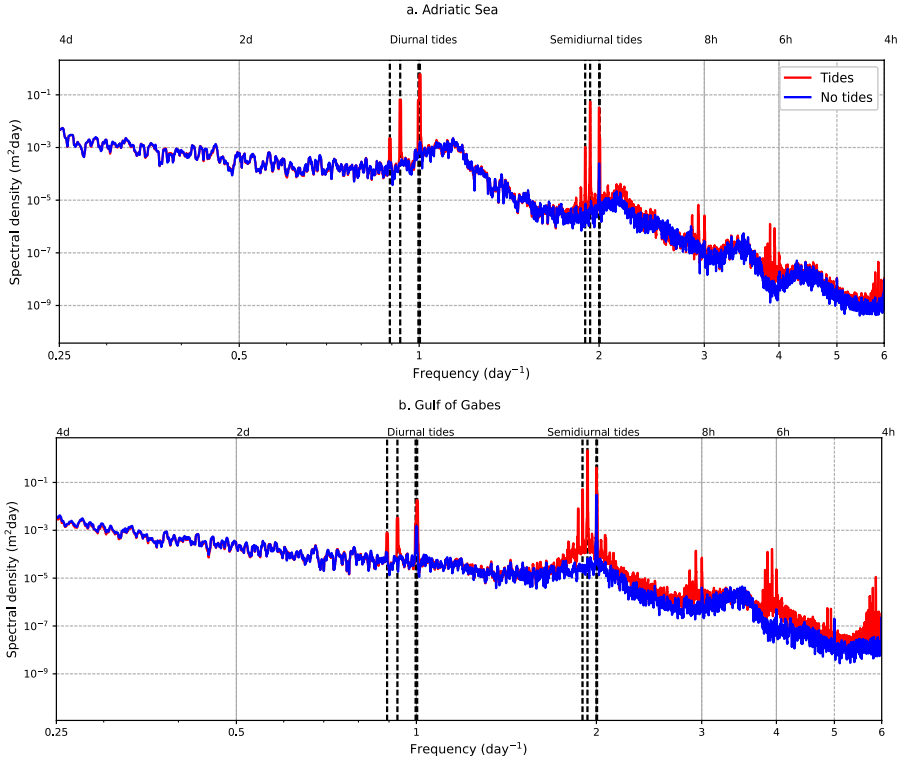

Figure 3. Energy density spectra of hourly mean sea surface height in the Mediterranean Sea for the period 2017-2021, for the model without tides (blue) and with tides (red), in a. Adriatic Sea, and b. Gulf of Gabes. An area-weighted mean was taken for each of the sub-basins.

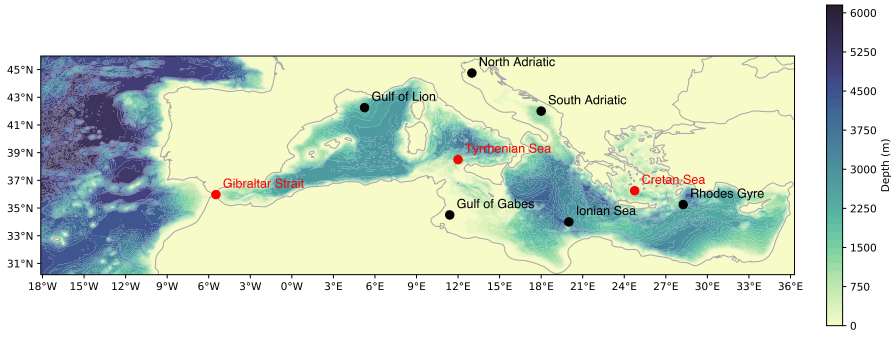

Figure 4. Map of selected points in the Mediterranean Sea. Points in red are discussed in this manuscript, while points in black are presented in the supplementary material.

Figure 4. From this, three contrasting points were selected to be shown in this work: the Gibraltar Strait, the Tyrrhenian Sea, and the Cretan Sea. Results for other points are available in the supplementary material.

https://doi.org/10.5194/egusphere-2023-2251
Preprint. Discussion started: 24 October 2023
© Author(s) 2023. CC BY 4.0 License.

We first calculate the rotary spectra for depth-averaged (barotropic) horizontal velocities (Fig. 5), for both clockwise and counter-clockwise components and then combine these to create the rotary kinetic energy density spectra. In the Gibraltar Strait (Fig. 5a), tides enhance kinetic energy at all frequencies, particularly at frequencies close to and higher than 12 hours. The basin mode frequency of 8.4 hours is enhanced by tides, and a peak at around 6h is also visible, which is due to nonlinear tidal effects (Palma et al., 2020). The Tyrrhenian Sea and Cretan Sea, unlike Gibraltar, have broad peaks at the near-inertial frequencies. Peaks at diurnal tidal frequencies are more apparent in the Tyrrhenian than in the Cretan Sea.

The spectra of kinetic energy density were split into vertical levels to consider baroclinic currents and internal wave modes. We note that upper layer currents (0-150m) are characterised by the entering Atlantic Water layer dynamics, while the intermediate layer (150-500m) currents are on average in the opposite direction to the surface, characterising the Intermediate Water circulation in the basin. We now analyse the effects of tides on this anti-estuarine zonally oriented conveyor belt described in Pinardi et al. (2019). Figure 6 shows spectra for the three selected points throughout the water column.

In the Gibraltar Strait, it is clear that the entire structure of kinetic energy is dominated by tides: tides enhance kinetic energy at all frequencies and depths. Internal tides are also seen in this region: Figure 6b shows peaks in kinetic energy at around 100m at the M2 and K1 tidal frequencies, implying the existence of internal tides as already shown by Gonzalez (2023). Some diurnal internal tidal energy is visible in the Tyrrhenian Sea (Fig. 6d), as well as a shift in the near-inertial peak when compared to the experiment without tides (Fig. 6c). The interaction of tides with near-inertial waves is clearer in the Cretan Sea (Fig. 6f), as the peak is shifted to a higher frequency compared to Fig. 6e.

To visualise the internal tidal motion in the basin, we use Hovmoller diagrams for one month (May 2019) hourly zonal currents for each of the selected points (Figs. 7-9). These provide a representation of the zonal conveyor cell of the Mediterranean Sea, composed, on average, of eastward currents in the first 150m and westward currents in the lower water column (Pinardi et al., 2019).

The three contrasting regions of the Mediterranean basin highlight the varying importance of tides, internal tides, and their interactions with near-inertial internal waves in different regions. While the Gibraltar Strait (Fig. 7) is dominated by semidiurnal tides, the other two regions (Figs. 8-9) show propagating near-inertial waves (Cozzani, 2023) interacting with internal tides, particularly in the Cretan Sea.

Internal tides are known to have large ageostrophic vertical velocities (Niwa and Hibiya, 2001; Li and von Storch, 2020) and thus an analysis of the vertical motion is mandatory. Figures 10-12 show the same month (May 2019) as Figs. 7-9, but this time looking at hourly vertical velocity. In Fig. 10 the Gibraltar Strait location shows a dominant vertical velocity oscillation at 12h. Contrastingly, inertial waves have greater importance in the Cretan Sea (Fig. 12) and they propagate downwards through the water column, notably around day 10-15 of the month and at 150-500m (Fig. 12d). The effect of tides on this is shown in Fig. 12e, where interactions between the internal tidal and near-inertial waves create wave-wave patterns during the same period. The Tyrrhenian Sea (Fig. 11) also has both near-inertial waves and internal tides at these depths, but the interaction here is weaker.

An interesting feature, shown in Figs. 10-12, is the baroclinic structure of the vertical velocity in the experiment with and without tides. Two zero crossings appear, one approximately at 150m, the lower limit of the inflowing branch of the zonal

https://doi.org/10.5194/egusphere-2023-2251
Preprint. Discussion started: 24 October 2023
© Author(s) 2023. CC BY 4.0 License.

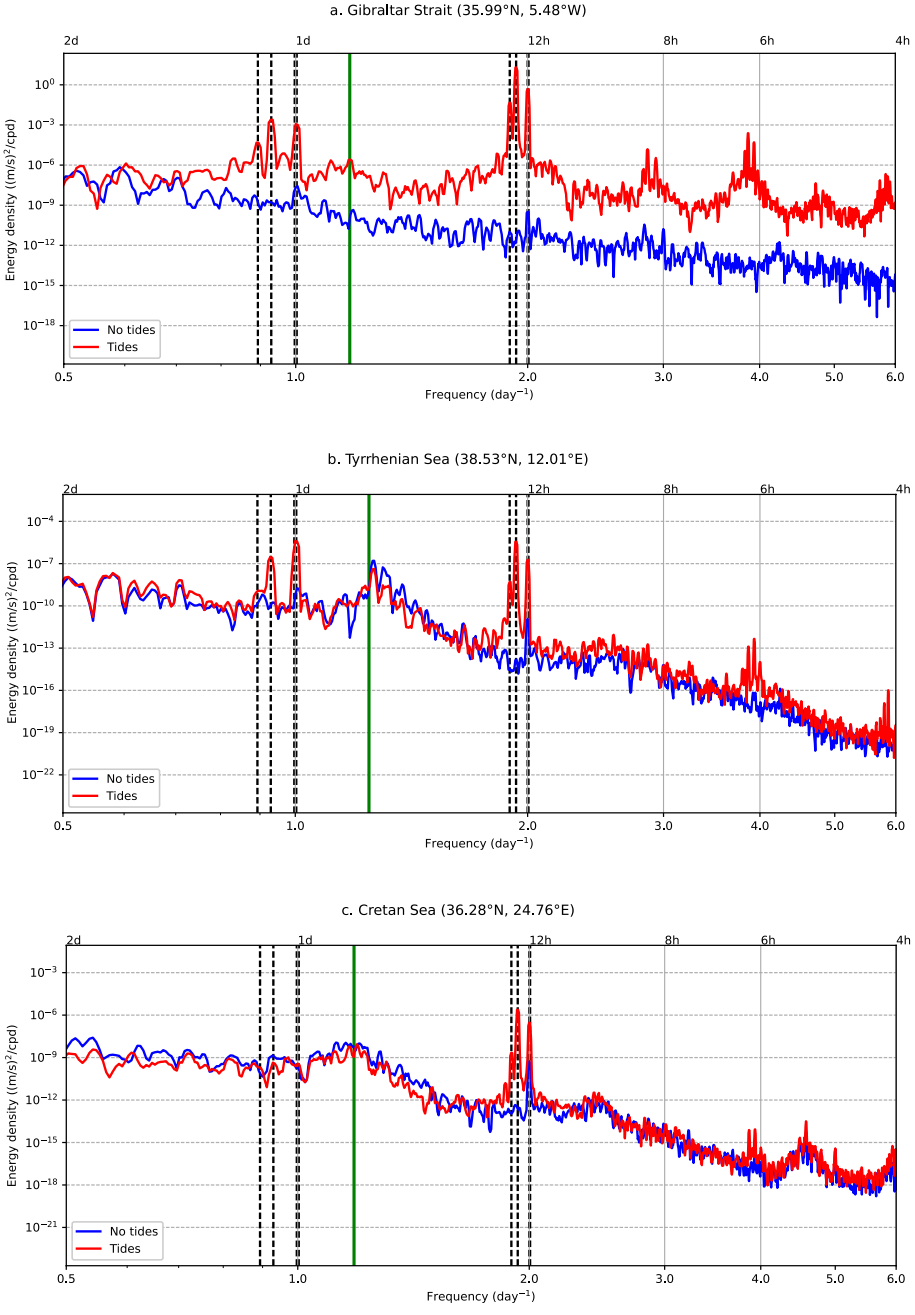

Figure 5. Barotropic rotary kinetic energy density spectra for points in a. Gibraltar Strait (35.99°N, 5.48°W), b. Tyrrhenian Sea (38.53°N, 12.01°E), and c. Cretan Sea (36.28°N, 24.76°E), with the tidal experiment in red and the experiment without tides in blue, using hourly outputs over six months, January-June 2019. Dashed lines represent the eight tidal components used in the model, and the green line is the inertial frequency. The locations of these points are shown in Figure 4.

https://doi.org/10.5194/egusphere-2023-2251
Preprint. Discussion started: 24 October 2023
© Author(s) 2023. CC BY 4.0 License.

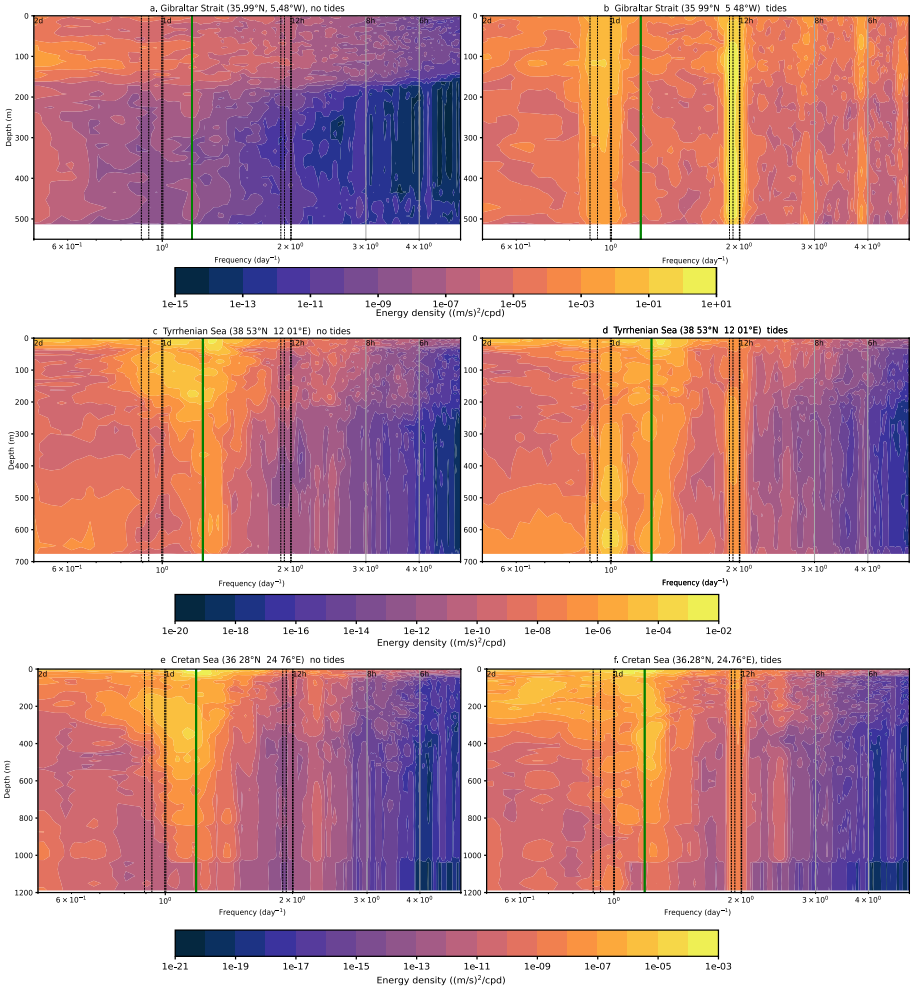

Figure 6. Rotary spectra of kinetic energy density over the full water column without tides at a. Gibraltar Strait (35.99°N, 5.48°W), c. Tyrrhenian Sea (38.53°N, 12.01°E), and e. Cretan Sea (36.28°N, 24.76°E), and with tides at b. Gibraltar Strait, d. Tyrrhenian Sea, and f. Cretan Sea. All data are for May 2019. The locations of these points are shown in Figure 4.

conveyor belt already described above (Pinardi et al., 2019), and the second at 300m. This is particularly apparent in the Gibraltar Strait (Fig. 10).

5 Mixed layer depth and water mass formation

Assessing the impact of tides on the mixed layer depth is indirect evidence of the importance of internal tides on the vertical mixing and vertical velocities. The mixed layer depth is calculated via a density criterion based on a density change of 0.01 kgm^{-3} (de Boyer Montégut et al., 2004). Figure 13 shows the change in winter (December-March) mixed layer depth in the

https://doi.org/10.5194/egusphere-2023-2251
Preprint. Discussion started: 24 October 2023
© Author(s) 2023. CC BY 4.0 License.

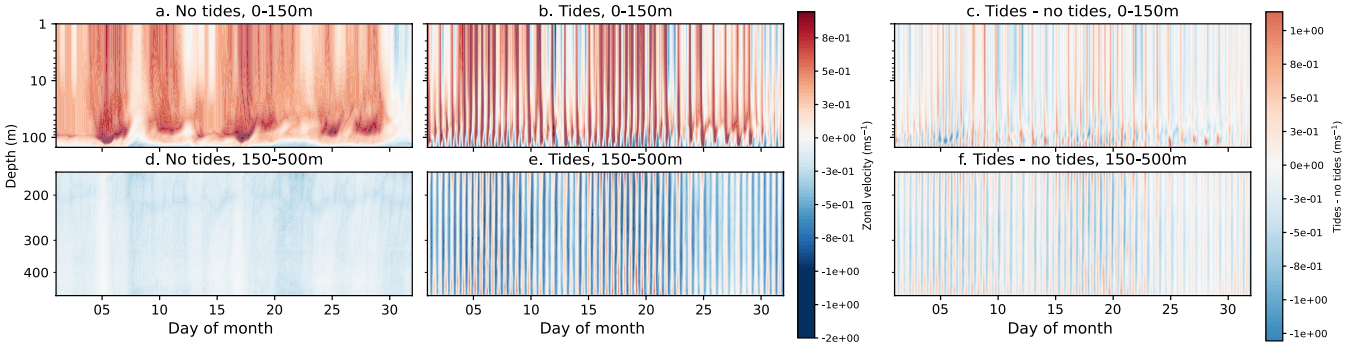

Figure 7. Hovmoller plots of depth against time of hourly mean zonal currents at a point in the Gibraltar Strait (35.99°N, 5.48°W, see Figure 4) in May 2019, for a. Model without tides, 0-150m, b. Tidal model, 0-150m, c. Tidal model – model without tides, 0-150m, d. Model without tides, 150-500m, e. Tidal model, 150-500m, f. Tidal model – model without tides. Note that the depth scale is logarithmic

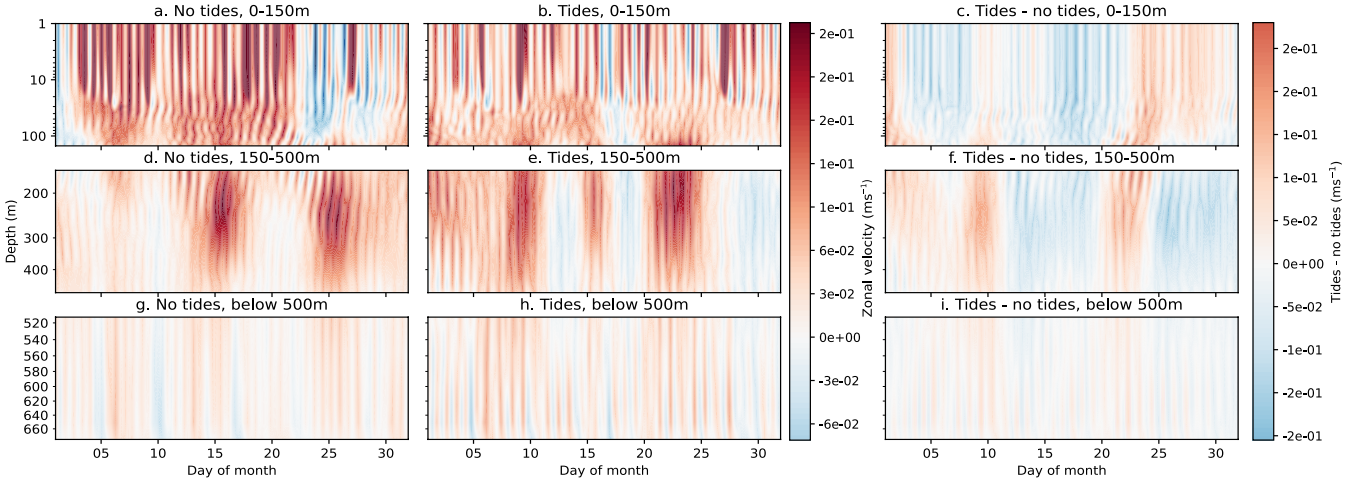

Figure 8. Hovmoller plots of depth against time of hourly mean zonal currents at a point in the Tyrrhenian Sea (38.53°N, 12.01°E, see Figure 4) in May 2019, for a. Model without tides, 0-150m, b. Tidal model, 0-150m, c. Tidal model – model without tides, 0-150m, d. Model without tides, 150-500m, e. Tidal model, 150-500m, f. Tidal model – model without tides, g. Model without tides, below 500m, h. Tidal model, below 500m, i. Tidal model – model without tides, below 500m. Note that the depth scale is logarithmic.

two experiments. There is an increase in mixed layer depth with tides throughout most of the basin, with notable exceptions in the Gibraltar Strait/Alboran Sea region, and in parts of the Aegean Sea. However, the biggest change occurs in the Gulf of
175 Lion region, a key area for the formation of deep water (Western Mediterranean Deep Water, WMDW, Fig. 1). A secondary large change occurs in the southern Adriatic Sea formation area (the Eastern Mediterranean Deep Water, EMDW, Fig. 1).

Increased mixed layer depth can be an indicator for increased dense water formation, but a direct analysis of this is needed to confirm whether tides are enhancing water mass formation as well as mixed layer depth. Pinardi et al. (2015) defined that intermediate water has densities of 29.1-29.2kgm^{-3} and deep water has densities greater than 29.2kgm^{-3}. Figure 14 shows

https://doi.org/10.5194/egusphere-2023-2251
Preprint. Discussion started: 24 October 2023
© Author(s) 2023. CC BY 4.0 License.

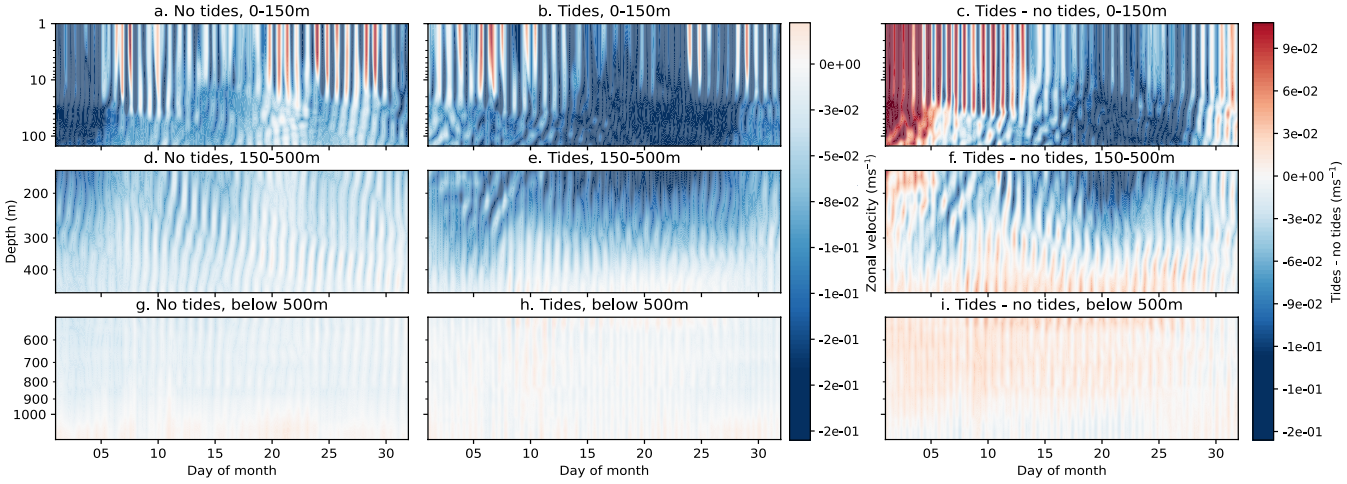

Figure 9. Hovmoller plots of depth against time of hourly mean zonal currents at a point in the Cretan Sea (36.28°N, 24.76°E, see Figure 4) in May 2019, for a. Model without tides, 0-150m, b. Tidal model, 0-150m, c. Tidal model – model without tides, 0-150m, d. Model without tides, 150-500m, e. Tidal model, 150-500m, f. Tidal model – model without tides, g. Model without tides, below 500m, h. Tidal model, below 500m, i. Tidal model – model without tides, below 500m. Note that the depth scale is logarithmic.

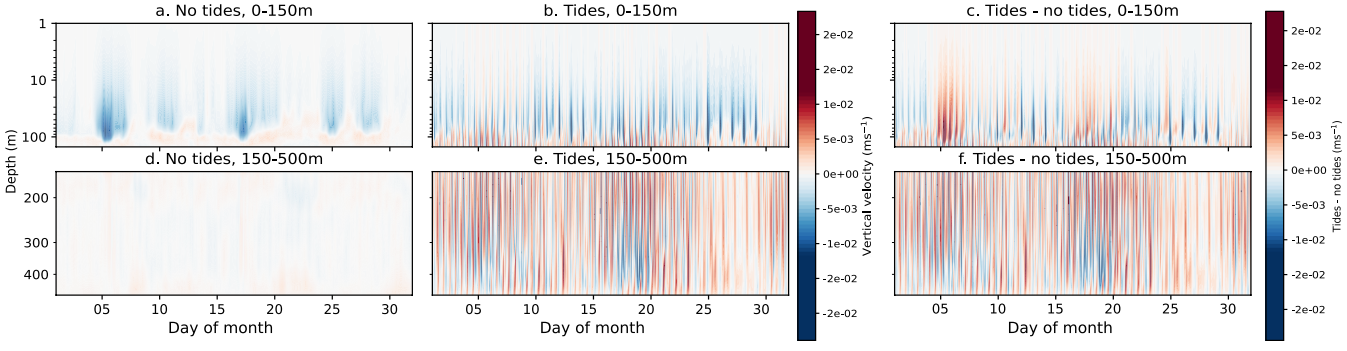

Figure 10. Hovmoller plots of depth against time of hourly mean vertical velocity at a point in the Gibraltar Strait (35.99°N, 5.48°W, see Figure 4) in May 2019, for a. Model without tides, 0-150m, b. Tidal model, 0-150m, c. Tidal model – model without tides, 0-150m, d. Model without tides, 150-500m, e. Tidal model, 150-500m, f. Tidal model – model without tides. Note that the depth scale is logarithmic.

the water mass formation rate in the deep and intermediate formation areas of Fig. 1 for each winter of the analysed period, with and without tides. The most notable change is in WMDW, which had a significant event in 2019, where the water mass formation rate was greatly increased in the tidal experiment. This is in agreement with Naranjo et al. (2014) showing that enhanced WMDW formation occurred with tides in four out of the five years analysed. Modest increases are also seen in LIW formation. EMDW and LDW have increased water mass formation rate when including tides in some years, and decreased in other years. We argue that this irregular behaviour is connected to the impact of tides on the strength of the pre-conditioning factors and the air-sea interaction heat fluxes that are affected by tides (Oddo et al., 2023).

https://doi.org/10.5194/egusphere-2023-2251
Preprint. Discussion started: 24 October 2023
© Author(s) 2023. CC BY 4.0 License.

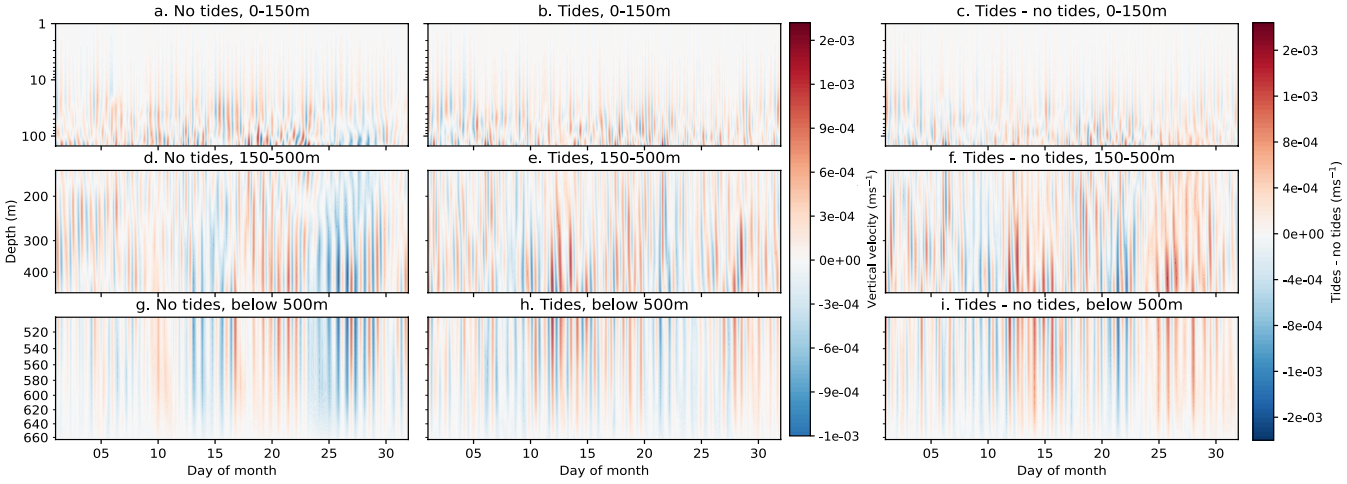

Figure 11. Hovmoller plots of depth against time of hourly mean vertical velocity at a point in the Tyrrhenian Sea (38.53°N, 12.01°E, see Figure 4) in May 2019, for a. Model without tides, 0-150m, b. Tidal model, 0-150m, c. Tidal model – model without tides, 0-150m, d. Model without tides, 150-500m, e. Tidal model, 150-500m, f. Tidal model – model without tides, g. Model without tides, below 500m, h. Tidal model, below 500m, i. Tidal model – model without tides, below 500m. Note that the depth scale is logarithmic.

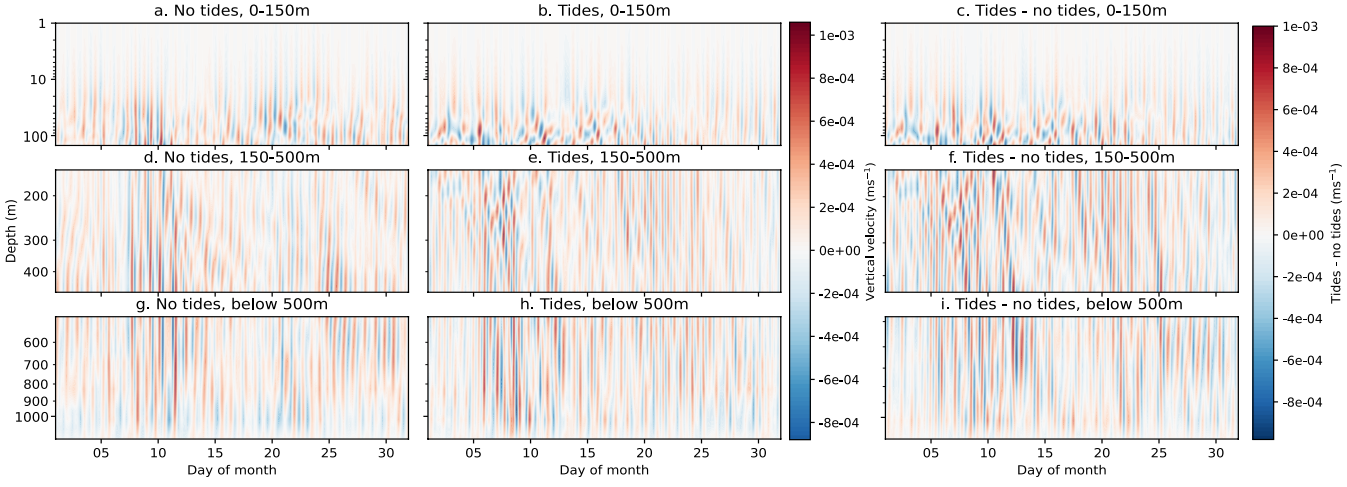

Figure 12. Hovmoller plots of depth against time of hourly mean vertical velocity at a point in the Cretan Sea (36.28°N, 24.76°E, see Figure 4) in May 2019, for a. Model without tides, 0-150m, b. Tidal model, 0-150m, c. Tidal model – model without tides, 0-150m, d. Model without tides, 150-500m, e. Tidal model, 150-500m, f. Tidal model – model without tides, g. Model without tides, below 500m, h. Tidal model, below 500m, i. Tidal model – model without tides, below 500m. Note that the depth scale is logarithmic.

https://doi.org/10.5194/egusphere-2023-2251
Preprint. Discussion started: 24 October 2023
© Author(s) 2023. CC BY 4.0 License.

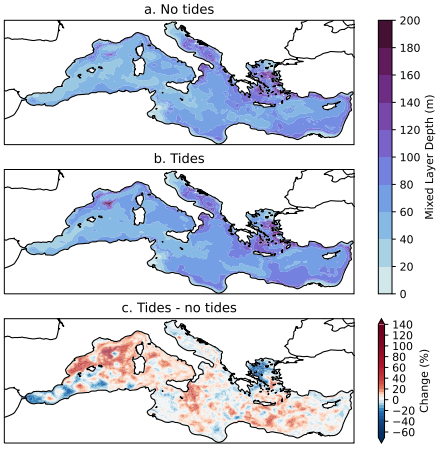

Figure 13. Winter (December-March) mean mixed layer depth in the Mediterranean Sea, for a. experiment without tides, b. experiment with tides, and c. the percentage difference between the tidal and non-tidal experiments.

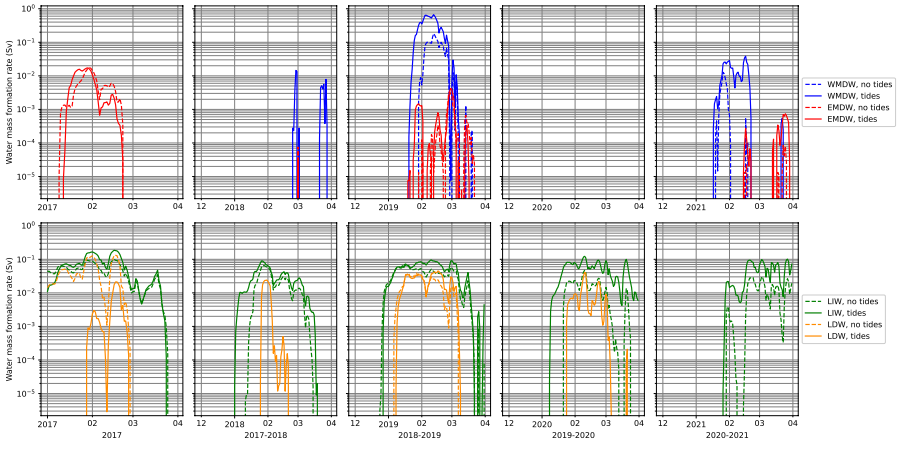

Figure 14. Daily water mass formation rate in winter 2017-2021, for the tidal experiment (solid lines) and the non-tidal experiment (dashed lines). Four types of water mass are included: Western Mediterranean Deep Water (blue), Eastern Mediterranean Deep Water (red), Levantine Intermediate Water (green), and Levantine Deep Water (orange).

6 Temperature and salinity

The salinity and temperature of the Mediterranean Sea are affected by tides, primarily in the upper layers above 150m, as can be seen in Figure 15. This is the layer affected by the Atlantic water and generally connected to the entering low salinity Atlantic water. As indicated in work by Naranjo et al. (2014) and Harzallah et al. (2016), inflowing salinity at Gibraltar increases when

https://doi.org/10.5194/egusphere-2023-2251
Preprint. Discussion started: 24 October 2023
© Author(s) 2023. CC BY 4.0 License.

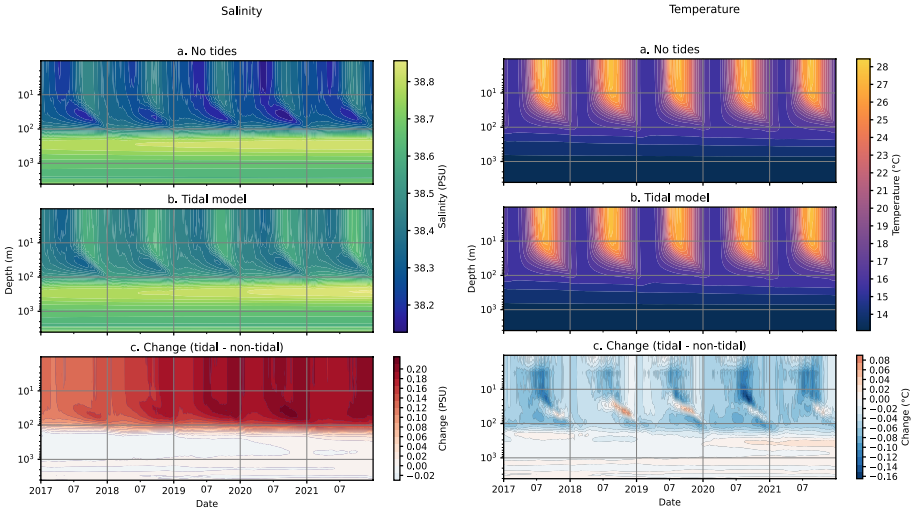

Figure 15. Hovmoller plot of depth against time of daily salinity (left) and temperature (right) in the Mediterranean Sea in 2017-2021, for the model without tides (a), with tides (b), and change (c): tidal model – model without tides. Note that the depth scale is logarithmic.

tides are introduced and upper layer temperature decreases, albeit by a smaller amount. This increase has a trend that does not stabilise in the few years of our experiment. This was also found by Harzallah et al. (2016), where the salinity difference between the experiments with and without tides increased for several decades before stabilising, since this stabilisation depends on the overturning time scales of the basin that could require several decades to spin up in full.

The additional increased salinity in the Mediterranean Sea due to tides and its trend over time can be compared to observations from profiling floats to understand whether the salinity increase follows the observational trend or it is overestimated. This was calculated for the Mediterranean Sea and integrated along vertical layers for each year in the experiment. Figure 16 shows the mean salinity bias and Root Mean Square Error (RMSE) of the experiments with respect to observations averaged in the whole basin and provided along nine vertical layers. It is shown that for the tidal experiment, the bias is generally negative in the surface layers and becomes positive below 60m, and does not present a clear linear trend and it varies by individual year. The lack of linear trend is also apparent in the non-tidal experiment, but there the salinity bias is positive throughout the upper layer. Overall the RMSE of the two experiments is similar in some years, but in 2019 and 2020, the tidal experiment has a much lower salinity bias in the upper layers. Figures 16c and d demonstrate that in both experiments the model error is larger at the surface up to 150m and is reduced to less than 0.15 PSU below this layer, where it also shows a lower temporal variability. Lower layers remain stable with small errors, whereas the surface varies more and produces larger errors when compared to observations.

https://doi.org/10.5194/egusphere-2023-2251
Preprint. Discussion started: 24 October 2023
© Author(s) 2023. CC BY 4.0 License.

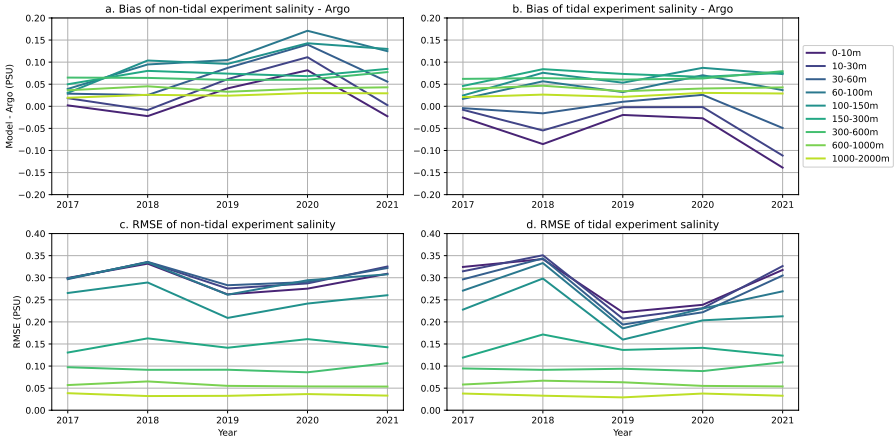

Figure 16. Salinity difference between the experiments and data from profiling floats for each analysed year (2017-2021), across nine layers for the Mediterranean Sea, presented as a. non-tidal experiment bias, b. tidal experiment bias, c. non-tidal experiment root mean square error, and d. tidal experiment root mean square error.

Experiment	Inflow	Outflow	Net Transport
Model without tides	0.85 Sv	-0.80 Sv	0.045 Sv
Tidal model	0.88 Sv	-0.84 Sv	0.043 Sv
Observations (Soto-Navarro et al., 2010)	0.81±0.06 Sv	-0.78±0.05 Sv	0.038±0.007 Sv

Table 3. Mass transport at the 5.48°W section of the Gibraltar Strait in the experiment without tides, tidal experiment, and observations from Soto-Navarro et al. (2010). Values for model outputs are calculated as mean inflow and outflow transport in the Gibraltar Strait for the period 2017-2021.

7 The Gibraltar Strait

Mass transport at the Gibraltar Strait is affected by tides, as was shown by Gonzalez (2023), Harzallah et al. (2016), and Naranjo et al. (2014). The effects of tides on the Gibraltar Strait mass transport are detailed in Table 3. Although the net transport in the Gibraltar Strait is not largely affected by tides, both the inflow and outflowing transport are increased by tides. Within observational errors we cannot fully distinguish between the tide and no-tide experiments, but we can estimate a 5-10% larger inflow/outflow transport with respect to literature. We argue that this is due to the relatively coarse resolution of the model in the Gibraltar Strait, where Gonzalez (2023) recently demonstrated that the required resolution for an accurate representation of the Gibraltar Strait would be about five times the one used in our model.

https://doi.org/10.5194/egusphere-2023-2251
Preprint. Discussion started: 24 October 2023
© Author(s) 2023. CC BY 4.0 License.

8 Conclusions

The effects of tides on the Mediterranean Sea circulation were studied through a twin numerical experiment approach based on a high-resolution (around 4km) model of the region, with and without the explicit representation of tides. Spectra of sea surface height and kinetic energy in the basin, as well as in key regions characterised by basin modes, revealed that the effects of tides on the energetics of the Mediterranean Sea extend far beyond the spatial and temporal scales of the tides themselves.

Tides enhance the power at 8h and 6h frequencies due to their nonlinear effects across the Mediterranean basin, amplifying the basin modes, as shown in the Sicily Strait by Palma et al. (2020). Tides also interact and amplify the other basin modes at 11.4h, 8.4h, and 7.4h, as well as the Adriatic modes at 10.7h and 6.7h, and the mode in the Gulf of Gabes at 8.2h. The Adriatic modes at 12h and 21.9h are visible in both the tidal and non-tidal experiments, but the 12h frequency is enhanced by tides. Results such as these demonstrate the complexity and non-linearity of tidal effects in the Mediterranean Sea.

The study then discussed the rotary spectra of the barotropic and full kinetic energy in several selected points in the Mediterranean Sea. This analysis showed the ubiquitous field of internal waves below around 150 meters, both at diurnal and semi-diurnal time frequencies. The Hovmoller diagram of zonal and vertical velocity components revealed the internal tide field structure in the basin, as well as the interaction of internal tides with near-inertial waves in some regions, such as the Cretan Sea. In addition to near inertial waves, both the semidiurnal and diurnal internal tides have high energy, potentially at an overall Mediterranean scale not previously highlighted.

Tides affect the mixed layer depth of the basin, with different signs in different regions. The Mediterranean deep and intermediate water formation is enhanced by tides in the Gulf of Lion, the WMDW region, and in the Levantine Sea where intermediate water masses are formed. This aligns with increases in the winter mixed layer depth across most of the Mediterranean Sea.

Further work in this area should include process-oriented studies of some features in the Mediterranean Sea that were discovered by this work, but that are subregional structures. The current literature lacks an up-to-date study calculating the barotropic oscillations of the Mediterranean Sea using a state-of-the-art numerical model. A more detailed study focusing on the region of formation and propagation of internal tides throughout the entire Mediterranean is lacking. In addition, a deeper focus on the impacts of tides, both barotropic and baroclinic, on vertical motion in the most vertically dynamic regions of the Mediterranean Sea would further help in understanding the overturning circulation in the basin. This could include considering the impact of tides on vertical mixing in deep and intermediate water formation regions, and how parametrization choices in numerical models may affect this.

Author contributions. BM ran the numerical models, analysed the results, and wrote the manuscript. EC and AG provided support in the set-up and running of the numerical models and analysis. NP planned the study and supported the analysis of model results. All authors reviewed and edited the manuscript.

Competing interests. The authors declare that they have no conflicts of interest.

https://doi.org/10.5194/egusphere-2023-2251
Preprint. Discussion started: 24 October 2023
© Author(s) 2023. CC BY 4.0 License.

Acknowledgements. This study has been conducted including support from the University of Bologna Ph.D. programme in Future Earth, Climate Change, and Societal Challenge, and the EU Copernicus Marine Service for the Mediterranean Monitoring and Forecasting Center.

https://doi.org/10.5194/egusphere-2023-2251
Preprint. Discussion started: 24 October 2023
© Author(s) 2023. CC BY 4.0 License.

References

Agresti, V.: Effects of tidal motion on the Mediterranean Sea General Circulation, Ph.D. thesis, Alma Mater Studiorum University of Bologna, https://doi.org/10.6092/unibo/amsdottorato/8516, 2018.

Arbic, B. K.: Incorporating tides and internal gravity waves within global ocean general circulation models: A review, Progr. Oceanogr., 206, https://doi.org/10.1016/j.pocean.2022.102824, 2022.

Armi, L. and Farmer, D.: The internal hydraulics of the Strait of Gibraltar and associated sills and narrows, Oceanol. Acta, 8, 37–46, 1985.

Candela, J., Winant, C., and Ruiz, A.: Tides in the Strait of Gibraltar, J. Geophys. Res. Oceans, 95, 7313–7335, https://doi.org/10.1029/JC095iC05p07313, 1990.

Clementi, E., Aydogdu, A., Goglio, A. C., Pistoia, J., Escudier, R., Drudi, M., Grandi, A., Mariani, A., Lyubartsev, V., Lecci, R., Cretí, S., Coppini, G., Masina, S., and Pinardi, N.: Mediterranean Sea Physical Analysis and Forecast (CMEMS MED-Currents, EAS6 system), Copernicus Monitoring Environment Marine Service (CMEMS), https://doi.org/10.25423/CMCC/MEDSEA_ANALYSISFORECAST_PHY_006_013_EAS6, 2021.

Coppini, G., Clementi, E., Cossarini, G., Salon, S., Korres, G., Ravdas, M., Lecci, R., Pistoia, J., Goglio, A. C., Drudi, M., Grandi, A., Aydogdu, A., Escudier, R., Cipollone, A., Lyubartsev, V., Mariani, A., Cretì, S., Palermo, F., Scuro, M., Masina, S., Pinardi, N., Navarra, A., Delrosso, D., Teruzzi, A., Di Biagio, V., Bolzon, G., Feudale, L., Coidessa, G., Amadio, C., Brosich, A., Miró, A., Alvarez, E., Lazzari, P., Solidoro, C., Oikonomou, C., and Zacharioudaki, A.: The Mediterranean forecasting system. Part I: evolution and performance, EGUsphere, pp. 1–50, https://doi.org/10.5194/egusphere-2022-1337, 2023.

Cozzani, E.: Oceanic near-inertial internal waves generation, propagation, and interaction with mesoscale eddies, Ph.D. thesis, Alma Mater Studiorum University of Bologna, 2023.

de Boyer Montégut, C., Madec, G., Fischer, A. S., Lazar, A., and Iudicone, D.: Mixed layer depth over the global ocean: An examination of profile data and a profile-based climatology, J. Geophys. Res., 109, https://doi.org/10.1029/2004JC002378, 2004.

de Lavergne, C., Vic, C., Madec, G., Roquet, F., Waterhouse, A. F., Whalen, C. B., Cuypers, Y., Bouruet-Aubertot, P., Ferron, B., and Hibiya, T.: A Parameterization of Local and Remote Tidal Mixing, J. Adv. Modell. Earth Sys., 12, e2020MS002 065, https://doi.org/10.1029/2020MS002065, 2020.

Egbert, G. D. and Erofeeva, S. Y.: Efficient inverse modeling of barotropic ocean tides, J. Atmosph. Oceanic Tech., 19.2, 183–204, 2002.

Ferrari, R. and Wunsch, C.: The distribution of eddy kinetic and potential energies in the global ocean, Tellus, 62A, 92–108, https://doi.org/10.1111/j.1600-0870.2009.00432.x, 2010.

GEBCO Bathymetric Compilation Group 2014: The GEBCO_2014 Grid, version 20150318, NERC EDS British Oceanographic Data Centre NOC, www.gebco.net, 2014.

Gonzalez, N. M.: Modélisation multi-échelle du détroit de Gibraltar et de son rôle de régulateur du climat méditerranéen, Ph.D. thesis, Sciences de l'Univers, de l'Environnement et de l'Espace, University of Toulouse, 2023.

Harzallah, A., Alioua, M., and Li, L.: Mass exchange at the Strait of Gibraltar in response to tidal and lower frequency forcing as simulated by a Mediterranean Sea model, Tellus A: Dyn. Meteorol. Oceanogr., 66, 23 871, https://doi.org/10.3402/tellusa.v66.23871, 2016.

Lamy, A., Millot, C., and Molines, J. M.: Bottom Pressure and Sea Level Measurements in the Gulf of Lions, J. Phys. Oceanogr., 11, 394–409, https://doi.org/10.1175/1520-0485(1981)011<0394:BPASLM>2.0.CO;2, 1981.

Leder, N. and Orlić, M.: Fundamental Adriatic seiche recorded by current meters, Annales Geophysicae, 22, 1449–1464, 2004.

https://doi.org/10.5194/egusphere-2023-2251
Preprint. Discussion started: 24 October 2023
© Author(s) 2023. CC BY 4.0 License.

Lee, H.-C., Rosatib, A., and Spelman, M. J.: Barotropic tidal mixing effects in a coupled climate model: Oceanic conditions in the Northern Atlantic, Ocean Modell., 11, 464–477, https://doi.org/10.1016/j.ocemod.2005.03.003, 2006.

Li, Z. and von Storch, J.-S.: M2 internal-tide generation in STORMTIDE2, J. Geophys. Res. Oceans, 125, https://doi.org/10.1029/2019JC015453, 2020.

Lozano, C. J. and Candela, J.: The M2 tide in the Mediterranean Sea: Dynamic analysis and data assimilation, Oceanol. Acta, 18, 419–441, 1995.

Medvedev, I. P., Vilibić, I., and Rabinovich, A. B.: Tidal Resonance in the Adriatic Sea: Observational Evidence, J. Geophys. Res. Oceans, 125, e2020JC016 168, https://doi.org/10.1029/2020JC016168, 2020.

Mihanović, H., Orlić, M., and Pasarić, Z.: Diurnal thermocline oscillations driven by tidal flow around an island in the Middle Adriatic, J. Marine Sys., 78, S157–S168, https://doi.org/10.1016/j.jmarsys.2009.01.021, 2009.

Müller, M., Haak, H., Jungclaus, J., Sündermann, J., and Thomas, M.: The effect of ocean tides on a climate model simulation, Ocean Modell., 35, 304–313, https://doi.org/10.1016/j.ocemod.2010.09.001, 2010.

Naranjo, C., Garcia-Lafuente, J., Sannino, G., and Sanchez-Garrido, J.: How much do tides affect the circulation of the Mediterranean Sea? From local processes in the Strait of Gibraltar to basin-scale effects, Progress Oceanogr., 127, 108–116, https://doi.org/j.pocean.2014.06.005, 2014.

Niwa, Y. and Hibiya, T.: Numerical study of the spatial distribution of the M2 internal tide in the Pacific Ocean, J. Geophys. Res. Oceans, 106, 22 441–22 449, https://doi.org/10.1029/2000JC000770, 2001.

Oddo, P., Bonaduce, A., Pinardi, N., and Guarnieri, A.: Sensitivity of the Mediterranean Sea level to atmospheric pressure and free surface elevation numerical formulation in NEMO, Geosci. Model Dev., 7, 3001–3015, https://doi.org/10.5194/gmd-7-3001-2014, 2014.

Oddo, P., Poulain, P., Falchetti, S., Storto, A., and Zappa, G.: Internal tides in the central Mediterranean Sea: observational evidence and numerical studies, Ocean Dyn., 73, 145–163, https://doi.org/10.1007/s10236-023-01545-z, 2023.

Pacanowski, R. C. and Philander, S. G. H.: Parameterization of Vertical Mixing in Numerical Models of Tropical Oceans, J. Phys. Oceanogr., 11, 1443–1451, https://doi.org/10.1175/1520-0485(1981)011<1443:POVMIN>2.0.CO;2, 1981.

Palma, M., Iacono, R., Sannino, G., Bargagli, A., Carillo, A., Fekete, B. M., Lombardi, E., Napolitano, E., Pisacane, G., and Struglia, M. V.: Short-term, linear, and non-linear local effects of the tides on the surface dynamics in a new, high-resolution model of the Mediterranean Sea circulation, Ocean Dyn., 70, 935–963, https://doi.org/10.1007/s10236-020-01364-6, 2020.

Pettenuzzo, D., Large, W., and Pinardi, N.: On the corrections of ERA-40 surface flux products consistent with the Mediterranean heat and water budgets and the connection between basin surface total heat flux and NAO, J. Geophys. Res., 115, https://doi.org/10.1029/2009JC005631, 2010.

Pinardi, N., Zavatarelli, M., Adani, M., Coppini, G., Fratianni, C., Oddo, P., Simoncelli, S., Tonani, M., Lyubartsev, V., Dobricic, S., and Bonaduce, A.: Mediterranean Sea large-scale low-frequency ocean variability and water mass formation rates from 1987 to 2007: A retrospective analysis, Prog. Oceanogr., 132, 318–332, https://doi.org/10.1016/j.pocean.2013.11.003, 2015.

Pinardi, N., Cessi, P., Borile, F., and Wolfe, C. L.: The Mediterranean sea overturning circulation, J. Phys. Oceanogr., 49, 1699–1721, https://doi.org/10.1175/JPO-D-18-0254.1, 2019.

Schwab, D. J. and Rao, D. B.: Barotropic oscillations of the Mediterranean and Adriatic Seas, Tellus A, 35A, 417–427, https://doi.org/10.1111/j.1600-0870.1983.tb00216.x, 1983.

Shchepetkin, A. F. and McWilliams, J. C.: The regional oceanic modeling system (ROMS): a split-explicit, free-surface, topography-following-coordinate oceanic model, Ocean Modell., 9, 347–404, https://doi.org/10.1016/j.ocemod.2004.08.002, 2005.

https://doi.org/10.5194/egusphere-2023-2251
Preprint. Discussion started: 24 October 2023
© Author(s) 2023. CC BY 4.0 License.

Simmons, H. L., Jayne, S. R., St. Laurent, L. C., and Weaver, A. J.: Tidally driven mixing in a numerical model of the ocean general circulation, Ocean Modell., 6, 245–263, https://doi.org/10.1016/S1463-5003(03)00011-8, 2004.

Soto-Navarro, J., Criado-Aldeanueva, F., García-Lafuente, J., and Sánchez-Román, A.: Estimation of the Atlantic inflow through the Strait of Gibraltar from climatological and in situ data, J. Geophys. Res. Oceans, 115, https://doi.org/10.1029/2010JC006302, 2010.